

Effects of space sizes on the dispersion of cough-generated droplets from a walking person

Cite as: Phys. Fluids 32, 121705 (2020); doi: 10.1063/5.0034874

Submitted: 23 October 2020 • Accepted: 7 November 2020 •

Published Online: 15 December 2020








View Online



Export Citation



CrossMark

Zhaobin Li (李墨斌),^{1,2}  Hongping Wang (王洪平),^{1,2}  Xinlei Zhang (张鑫磊),^{1,2}  Ting Wu (吴霆),^{1,2} 
and Xiaolei Yang (杨晓雷)^{1,2,a)} 

AFFILIATIONS

¹The State Key Laboratory of Nonlinear Mechanics, Institute of Mechanics, Chinese Academy of Sciences, Beijing 100190, China

²School of Engineering Sciences, University of Chinese Academy of Sciences, Beijing 100049, China

Note: This paper is part of the Special Topic, Flow and the Virus.

^{a)}Author to whom correspondence should be addressed: xyang@imech.ac.cn

ABSTRACT

The dispersion of viral droplets plays a key role in the transmission of COVID-19. In this work, we analyze the dispersion of cough-generated droplets in the wake of a walking person for different space sizes. The air flow is simulated by solving the Reynolds-averaged Navier–Stokes equations, and the droplets are modeled as passive Lagrangian particles. Simulation results show that the cloud of droplets locates around and below the waist height of the manikin after 2 s from coughing, which indicates that kids walking behind an infectious patient are exposed to higher transmission risk than adults. More importantly, two distinct droplet dispersion modes occupying significantly different contamination regions are discovered. A slight change of space size is found being able to trigger the transition of dispersion modes even though the flow patterns are still similar. This shows the importance of accurately simulating the air flow in predicting the dispersion of viral droplets and implies the necessity to set different safe-distancing guidelines for different environments.

Published under license by AIP Publishing. <https://doi.org/10.1063/5.0034874>

COVID-19 can be transmitted via respiratory droplets when a person is close to a patient who is coughing or sneezing.¹ In this transmission process, the viral droplets expelled from the infectious host are transported and dispersed in the ambient air flow before finally being inhaled by a susceptible.² For this reason, social-distancing guidelines must be built based on a thorough understanding of the air flow and its influence on the droplet dispersion. The recommended distance could also vary in different circumstances. For example, a droplet dispersion range is found to be much extended in a cold and wet environment than under hot and dry conditions due to different evaporation rates.^{3,4} It has also been demonstrated that wearing a mask can effectively reduce the risk of infection via viral droplet dispersion.^{5,6} In an outdoor environment, wind is found being able to enhance the droplet traveling distance significantly, especially for small-size droplets.^{7,8} However, more attention should be paid to an indoor environment, where most transmission occurs due to space constraints and poor ventilation conditions.⁹

Previous studies have shown the influence of air-conditioners,^{10,11} glass barriers and windows in a classroom,¹² and the use of toilet¹³ on the spreading of viral droplets, among others. This work complements the current understanding of indoor viral droplet dispersion by combining both human motion and space constraints. More specifically, we analyze the dispersion of cough droplets behind a walking person using Computational Fluid Dynamics (CFD), focusing on the influence of the indoor space constraints on the dispersion by conducting simulations with different space sizes. The results reveal that the pattern of droplet dispersion can be significantly altered by only a slight change in the air flow, which demonstrates the importance of accurately predicting the air flow in predicting virus transmission for different environments.

The numerical investigation consists of two steps: (1) solve the flow around the walking person and (2) simulate the transient evolution of the cough droplets using the air flow obtained from step 1 through one-way coupling, i.e., the air flow is not affected by the

motion of the droplets. One-way coupling is generally valid when the volume fraction is less than 10^{-6} in particle-laden turbulent flows.¹⁴ For cough-generated flows, the volume fraction is in the range of 10^{-7} – 10^{-5} defined with the total saliva droplet volume to the expelled air volume.¹⁵ When defined with the volume of the air in the wake of a walking person, which is the scenario of interest in this work, the volume fraction will fall exactly into the one-way coupling range.

The air flow is simulated by solving the incompressible Reynolds-Averaged Navier–Stokes (RANS) equations as follows:

$$\nabla \cdot \mathbf{u} = 0, \tag{1}$$

$$\mathbf{u} \cdot (\nabla \mathbf{u}) = -\frac{\nabla p}{\rho} + \nu_{\text{eff}} \nabla^2 \mathbf{u}, \tag{2}$$

where \mathbf{u} denotes the velocity vector, p is the pressure, ρ is the density of air, and ν_{eff} is the effective viscosity, including both the molecular viscosity and the turbulent eddy viscosity computed with the k – ω SST turbulence model.¹⁶ The equations are discretized with the finite volume method and solved with the simpleFoam solver of OpenFOAM.¹⁷

The respiratory droplets are modeled as passive particles with three translational degrees of freedom. The rotation and evaporation of the droplets and interactions between droplets are excluded. The dispersion of the droplets is simulated using the Lagrangian method with their motion governed by the following equations:

$$\frac{d\mathbf{x}}{dt} = \mathbf{v}_c + \mathbf{v}_t, \tag{3}$$

$$m \frac{d\mathbf{v}_c}{dt} = m\mathbf{g} + \mathbf{F}, \tag{4}$$

where \mathbf{x} is the instantaneous position of the particle, \mathbf{v}_c is the computed particle velocity, \mathbf{v}_t is the stochastic velocity due to turbulence, m is the particle mass, \mathbf{g} is the gravity, and \mathbf{F} is the flow force acting on the particle, including the buoyancy and the drag computed with the air flow. The perturbation velocity \mathbf{v}_t is computed with the stochastic dispersion model of Gosman and Ioannides,¹⁸ where the fluctuation in direction i is computed as

$$v_t^i = \sigma \sqrt{\frac{2k}{3}}, \tag{5}$$

with $\sigma \sim N(0, 1)$ following the standard normal distribution and k is the turbulence kinematic energy obtained from the simulation of the air flow. The equations are solved with icoUncoupledKinematicParcelFoam of OpenFOAM.

It is noted that the dynamics at the droplet scale, such as the effect of droplet evaporation, is not considered in this work. Recently, Dbouk and Drikakis³ developed a new theory to predict the heat and mass transfer of virus contaminated saliva droplets and demonstrated that a cold or wet environment can prevent the droplet evaporation and help the virus survive. Based on this theory, the present evaporation-free configuration represents the most risky winter-like scenario.

A human-shape manikin is employed in the simulation, which contains details of the human body and clothes to represent a medium-built male with the height of 1.8 m and the shoulder

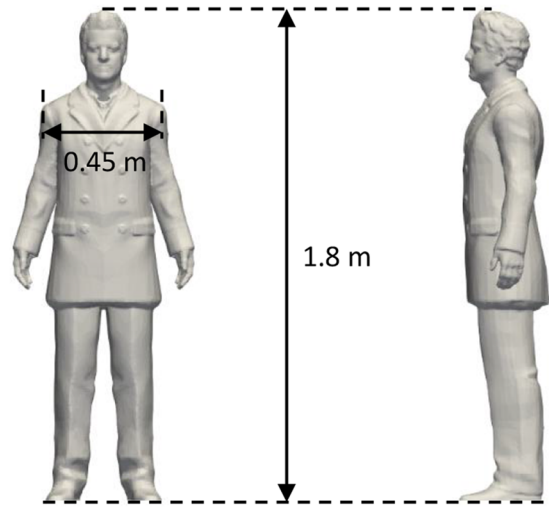


FIG. 1. The manikin used in the simulations.

breadth of 0.45 m, as shown in Fig. 1. To simplify the problem, the manikin is assumed as a rigid body without considering the motion of arms, legs, and other body parts relative to the overall movement.

The computational domain is rectangular with a central symmetric plane (see Fig. 2). The domain height is $H = 2.8$ m, the length in front of the manikin is $L_1 = 2.0$ m, and the length behind the manikin is $L_2 = 10.0$ m. Different domain breadths from $B = 1.2$ m to $B = 6.0$ m are considered to analyze the influence of space sizes. In the flow simulation, the reference frame is fixed to the manikin with air blowing from the inlet. A free-slip condition is imposed on the lateral, top, and bottom boundaries. A non-slip condition is imposed on the manikin with the nutUSpalding wall function in OpenFOAM.^{19,20} The background mesh is Cartesian with $\Delta h = 0.1$ m. Local refinement around the manikin is applied, and the center of the first layer cell is in the logarithmic region with $y^+ \approx 35$.

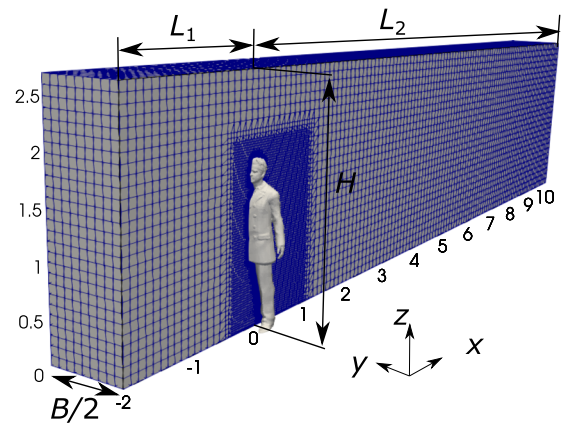


FIG. 2. Computational domain and mesh configuration.

The total number of cells is $\sim 0.7 \times 10^6$. The simulations represent a daily scenario where a man walks at a constant speed in the range of $U \in [1.2, 1.8]$ m/s and coughs. The Reynolds number based on the shoulder breadth and the walking speed is in the range of $Re \in [3.6 \times 10^4, 5.4 \times 10^4]$.

In this work, the droplets are modeled as a cloud of spheroid particles and are injected into the computational domain from the mouth of the manikin within 0.12 s at the beginning. The droplet diameter distribution follows the Weibull distribution. The diameter range is $d \in [1.0, 300.0]$ μm , and the mean diameter is 80.0 μm . The total number of droplets is 1008 with the total mass of 7.7 mg. All particles are emitted with a horizontal velocity of $v_c^x = 5.0$ m/s. These characteristics follow a recent CFD analysis of cough droplet dispersion.⁵ In the simulation of the droplet dispersion, the ground fixed reference frame is employed and the manikin moves from the right to the left. The manikin surface is modeled as a non-slip wall so that the droplets reaching the manikin remain attached afterward. The integration time step is fixed at $\Delta t = 5 \times 10^{-5}$ s. For each case, the computational time is ~ 50 min for the flow simulation and ~ 90 min for the simulation of droplet dispersion on a single-core processor of 3.6 GHz.

Figure 3 shows the flow field around the manikin for $B = 1.2$ m and 6.0 m with walking speed $U = 1.5$ m/s. In Figs. 3(a) and 3(e), the vertical dashed lines are 2 m away from the manikin. The small panels represent the flow field on horizontal planes and are clipped at 2 m downstream from the manikin to indicate the commonly practiced social-distancing. Panels on the left are for the case with $B = 1.2$ m, and those on the right are for the case with $B = 6.0$ m. In general, the manikin decelerates the flow around it as a bluff-body. However, the flow patterns are found being strongly related to the shape of the human body. As shown in Fig. 3(a), a reverse flow region exists behind the head and the torso with the maximum reverse velocity locating approximately at the waist-height ($z = 1.0$ m, marked by *c*). Behind the legs, the flow is slightly faster than the ambient flow. Figures 3(b)–3(d) show the wake behind the mouth, the waist, and the legs. As seen, the manikin’s torso part

[Fig. 3(c)] induces the strongest wake. Special wake patterns, such as the jets through the gaps between the hands and the torso [in Fig. 3(c)] and the gap between the legs [in Fig. 3(d)], are also remarkable, in which the latter one explains the high speed flow below the waist shown in Fig. 3(a). At 2 m downstream, the wake is almost negligible at the mouth height and the leg height as shown in Figs. 3(b) and 3(d), respectively, while it is still visible at the waist height as shown in Fig. 3(c). For the case with $B = 6.0$ m, similar flow patterns are observed in Figs. 3(e)–3(h), but with a slightly larger recirculation region behind the torso and a slightly stronger velocity deficit as compared with the case with $B = 1.2$ m.

Figures 4(a)–4(c) compare the transverse profiles of the stream-wise velocity in the wake between the cases with $B = 1.2$ m and 6.0 m at $U = 1.5$ m/s on the waist height. As seen, the differences manifest mostly in the near wake. At 1 m behind the manikin [Fig. 4(a)], the major difference exists in the velocity overshoot region outside the wake, where the streamwise velocity of the case with $B = 1.2$ m is $\sim 10\%$ larger than that of the case with $B = 6.0$ m. In Fig. 4(d), the vertical profiles of the streamwise velocity are compared. As seen, the two vertical profiles are similar to each other with complex variations and the largest velocity deficit located around the waist height. In both cases, the upper boundary of the wake region is approximately at 1.5 m above the ground at $x = 1$ m downstream of the manikin and gradually decreases at further downstream locations. Outside the wake in the vertical direction, the streamwise velocity is also higher for the case with $B = 1.2$ m because of the higher blockage effect due to the narrower space. Traveling downstream, the wake recovers with momentum exchange with the free stream in both cases, and the differences between the two cases become smaller, especially for the profiles in the transverse direction as shown in Fig. 4(c).

After showing the flow field, we examine the dispersion of droplets in Fig. 5 for five different instants. At $t = 0.1$ s, a small cloud of droplets, marked as red dots, releases from the manikin’s mouth. At $t = 1.0$ s, the cloud of droplets expands in size and advances at a velocity smaller than the manikin. For both cases, the cloud is of oval shape at $t = 1.0$ s from the side view, which is similar to the

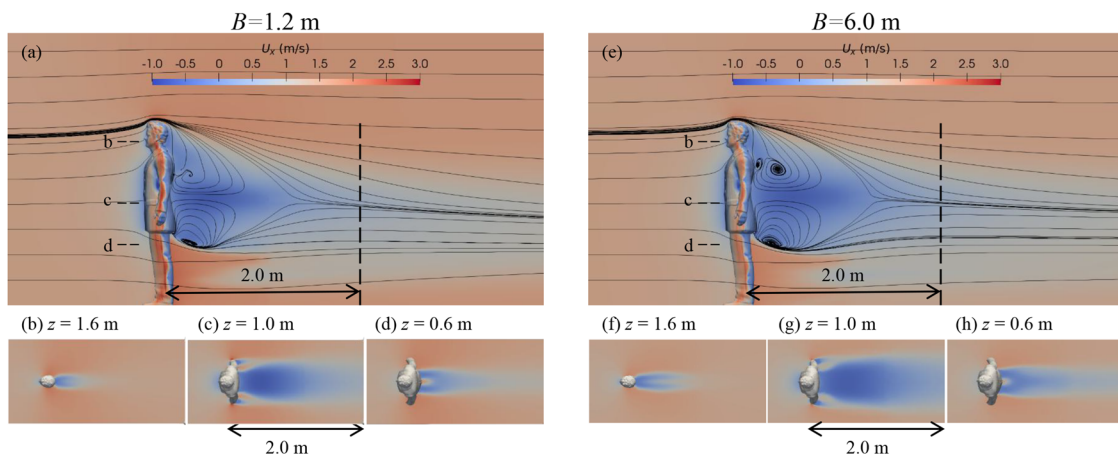


FIG. 3. Patterns of air flow around the manikin for the cases with $B = 1.2$ m [left, (a)–(d)] and $B = 6.0$ m [right, (e)–(h)] and walking speed 1.5 m/s. [(a) and (e)] Contours of streamwise velocity and streamlines on the symmetrical plane and [(b)–(d)] and [(f)–(h)] contours of streamwise velocity on horizontal planes located at different vertical locations.

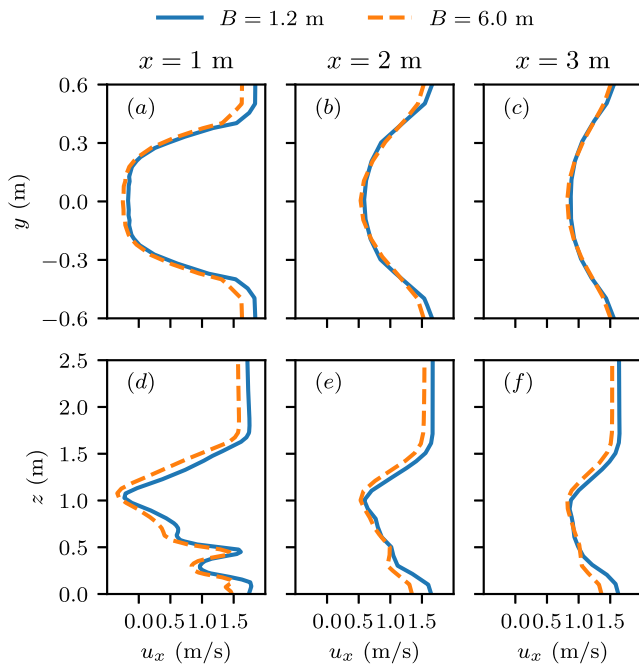


FIG. 4. Comparison of the streamwise velocity profile behind the manikin for the cases with $B = 1.2$ m and 6.0 m and manikin's walking speed 1.5 m/s with (a)–(c) for transverse profiles of the streamwise velocity u_x at the waist height $z = 1.0$ m, and (d)–(f) for vertical profiles of u_x on the symmetry plane.

simulation result of cough droplets carried by mild wind without a wake effect in the work of Dbouk and Drikakis.⁷ This similarity of the shape of the droplet cloud between the present work and that in the reference, in which the head is not considered, implies that the

head-induced wake has very limited effects on the droplet motion. The oval shape deformation of the droplet cloud can be explained as a result of different advancing and settling velocities of droplets of different sizes.²¹ At $t = 2.0$ s, the cloud drops approximately to the waist height and deforms into an elongated shape that expands horizontally for both cases. Significant differences between the two cases are observed starting from this instant. For the case with $B = 1.2$ m, the cloud is left further behind the manikin, and at $t = 5.0$ s, the cloud locates in the range of $x \in [2, 4]$ m, leaving the region just behind the manikin ($x \in [4, 7.5]$ m) nearly unaffected. In the case with $B = 6.0$ m, on the other hand, a part of the droplet cloud moves toward the manikin from $t = 1.0$ s to $t = 2.0$ s. From $t = 3.0$ s to 5.0 s, the left limit of the cloud catches up with the manikin and the droplet cloud extends in a region much broader than the case with $B = 1.2$ m.

These two significantly different patterns are referred to as the attached mode and the detached mode hereafter. In the case with $B = 6.0$ m, the attached mode is formed because a large portion of the droplets falls into the re-circulation bubble as shown in Fig. 5(b) in the snapshots at $t = 1.0$ s and 2.0 s. In the case with $B = 1.2$ m, on the other hand, the slightly larger overshoot velocity above the wake and the smaller re-circulation bubble help the droplets escape from the reverse flow region, forming the detached mode. A mode map for different space sizes (different B values) and different walking speeds (U) is shown in Fig. 6. As seen, the attached mode exists for most cases, while the detached mode is only observed for cases with narrower space and higher walking speed.

In summary, we investigated the effects of space sizes on the dispersion of cough droplets behind a walking manikin of realistic shape using the RANS method. Similar flow patterns are observed for cases with different space constraints. For all the considered cases, suspension of droplets is observed below the waist height of the manikin for distance larger than 2 m, indicating higher risks for kids who walk behind a coughing patient when following the

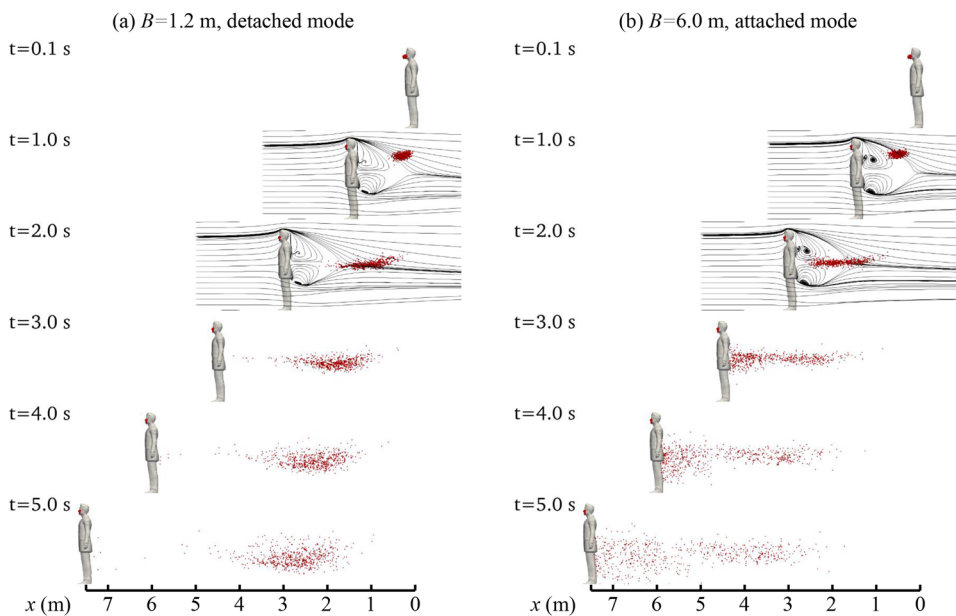


FIG. 5. Patterns of droplet dispersion in the wake of the walking manikin for (a) $B = 1.2$ m case and (b) $B = 6.0$ m case, with walking speed 1.5 m/s. Droplets are plotted as red dots of the same size, regardless of their real diameter. At $t = 1.0$ s and 2.0 s, the black streamlines are added to illustrate the range of the re-circulation bubbles.

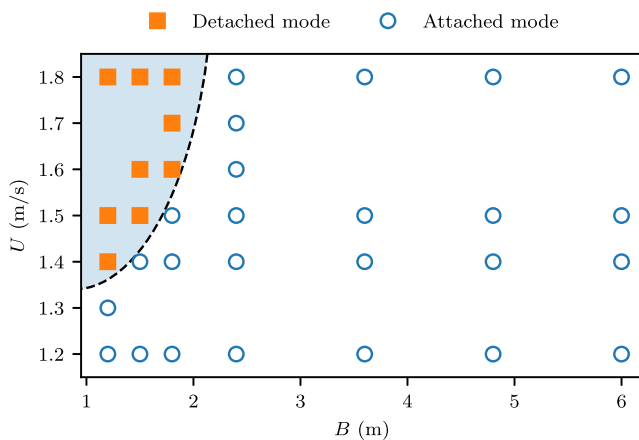


FIG. 6. The mode map in the two-dimensional space of the domain breadth B and the walking speed U .

current social-distancing guideline. More importantly, two distinct particle dispersion modes, i.e., the attached mode and the detached mode, are discovered for different space sizes. The detached mode only occurs for cases with small space and high walking speed, while the attached mode occurs for other cases. When the attached mode occurs, the cloud of droplets is observed starting from the rear of the manikin with elongated shape in the streamwise direction. For the detached mode, on the other hand, the cloud of droplets is separated from the manikin and convected at a much lower speed, with its size in the streamwise direction much smaller and the droplet concentration remarkably higher than that of the attached mode at 5 s after coughing. This poses a great challenge on determining the safe distance for places with high space constraint, e.g., in a very narrow corridor, as a person may still inhale viral droplets even the patient is far in front of him/her.

In this work, only the steady-state part of the air flow around the person is explicitly taken into account for the dispersion of droplets without considering the flow unsteadiness, and with the effect of turbulent fluctuations approximated with a kinematic model. Methods of higher fidelity, such as large-eddy simulation or direct numerical simulation,²² with the capacity to predict the unsteady and turbulent motion of the wake flow, could be employed in the future to study the present cases in more detail.

This work was partially supported by the NSFC Basic Science Center Program for “Multiscale Problems in Nonlinear Mechanics” (Grant No. 11988102).

DATA AVAILABILITY

The data that support the findings of this study are available from the corresponding author upon reasonable request.

REFERENCES

- W H Organization, “Modes of transmission of virus causing COVID-19: Implications for IPC precaution recommendations: Scientific brief, 27 March 2020,” Technical Report, World Health Organization, 2020.
- R. Mittal, C. Meneveau, and W. Wu, “A mathematical framework for estimating risk of airborne transmission of COVID-19 with application to face mask use and social distancing,” *Phys. Fluids* **32**, 101903 (2020).
- T. Dbouk and D. Drikakis, “Weather impact on airborne coronavirus survival,” *Phys. Fluids* **32**, 093312 (2020).
- B. Wang, H. Wu, and X.-F. Wan, “Transport and fate of human expiratory droplets—A modeling approach,” *Phys. Fluids* **32**, 083307 (2020).
- T. Dbouk and D. Drikakis, “On respiratory droplets and face masks,” *Phys. Fluids* **32**, 063303 (2020).
- S. Verma, M. Dhanak, and J. Frankenfield, “Visualizing the effectiveness of face masks in obstructing respiratory jets,” *Phys. Fluids* **32**, 061708 (2020).
- T. Dbouk and D. Drikakis, “On coughing and airborne droplet transmission to humans,” *Phys. Fluids* **32**, 053310 (2020).
- S. K. Das, J.-e. Alam, S. Plumari, and V. Greco, “Transmission of airborne virus through sneezed and coughed droplets,” *Phys. Fluids* **32**, 097102 (2020).
- H. Nishiura, H. Oshitani, T. Kobayashi, T. Saito, T. Sunagawa, T. Matsui, T. Wakita, MHLW Covid-19 Team, and M. Suzuki, “Closed environments facilitate secondary transmission of coronavirus disease 2019 (COVID-19),” [medRxiv:2020.02.28.20029272](https://doi.org/10.1101/2020.02.28.20029272) (2020).
- J. Lu, J. Gu, K. Li, C. Xu, W. Su, Z. Lai, D. Zhou, C. Yu, B. Xu, and Z. Yang, “COVID-19 outbreak associated with air conditioning in restaurant, Guangzhou, China, 2020,” *Emerging Infect. Dis.* **26**, 1628 (2020).
- B. Zhang, G. Guo, C. Zhu, Z. Ji, and C.-H. Lin, “Transport and trajectory of cough-induced bimodal aerosol in an air-conditioned space,” *Indoor Built Environ.* (published online 2020).
- M. Abuhegazy, K. Talaat, O. Anderoglu, and S. V. Poroseva, “Numerical investigation of aerosol transport in a classroom with relevance to COVID-19,” *Phys. Fluids* **32**, 103311 (2020).
- Y.-y. Li, J.-X. Wang, and X. Chen, “Can a toilet promote virus transmission? From a fluid dynamics perspective,” *Phys. Fluids* **32**, 065107 (2020).
- S. Elghobashi, “On predicting particle-laden turbulent flows,” *Appl. Sci. Res.* **52**, 309–329 (1994).
- L. Bourouiba, E. Dehandschoewercker, and J. W. M. Bush, “Violent expiratory events: On coughing and sneezing,” *J. Fluid Mech.* **745**, 537–563 (2014).
- F. R. Menter, “Two-equation eddy-viscosity turbulence models for engineering applications,” *AIAA J.* **32**, 1598–1605 (1994).
- See <https://www.openfoam.com/> for OpenCFD, OpenFOAM user guide; accessed 13 October 2020.
- A. D. Gosman and E. Ioannides, “Aspects of computer simulation of liquid-fueled combustors,” *J. Energy* **7**, 482–490 (1983).
- D. Spalding, “A single formula for the law of the wall,” *Trans. ASME, J. Appl. Mech.* **28**, 455–458 (1961).
- F. Liu, “A thorough description of how wall functions are implemented in OpenFOAM,” Technical Report, Chalmers University of Technology, Gothenburg Sweden, 2016.
- H. Wang, Z. Li, X. Zhang, L. Zhu, Y. Liu, and S. Wang, “The motion of respiratory droplets produced by coughing,” *Phys. Fluids* **32**, 125102 (2020).
- Z. Zhou, S. Wang, and G. Jin, “A structural subgrid-scale model for relative dispersion in large-eddy simulation of isotropic turbulent flows by coupling kinematic simulation with approximate deconvolution method,” *Phys. Fluids* **30**, 105110 (2018).